RSC Advances

PAPER

View Article Online
View Journal | View Issue

Cite this: *RSC Adv.*, 2015, **5**, 22712

Atomic layer deposition of Zn_3N_2 thin films: growth mechanism and application in thin film transistor

Soumyadeep Sinha,[a] Devika Choudhury,[a] Gopalan Rajaraman[b] and Shaibal K. Sarkar*[a]

Received 20th October 2014
Accepted 18th February 2015

DOI: 10.1039/c4ra12776e

www.rsc.org/advances

In this paper we present atomic layer deposition (ALD) of zinc nitride thin films using diethylzinc (DEZ) and ammonia (NH_3). Density Functional Theory (DFT) is used to calculate the atomistic reaction pathway. The self-limiting growth characteristic is verified at 315 °C. Saturated growth rate is found to be 0.9 Å per ALD cycle. The as deposited films are found to be polycrystalline with preferential orientation in the {321} direction. The performance of the material is further investigated as channel layer in thin film transistor (TFT) applications.

1. Introduction

Zinc nitride is a n-type semiconductor having low electron effective mass[1] (*ca.* $0.29m_0$, where m_0 is the free electron mass) and high carrier mobility (156 $cm^2\ V^{-1}\ s^{-1}$)[1,2] with large breakdown voltage.[3] Additionally, it has a wide direct bandgap and high refractive index (2.2–2.4).[4,5] These unique combinations of electrical and optical properties render zinc nitride as a prospective transparent conductor. Though not studied extensively, lately its applications in sensors[6] and thin film transistors (TFT)[2,7] have drawn considerable attention.

A variety of techniques are used to deposit zinc nitride thin films. Although gas phase depositions are moderately common, a few reports on solution phase electrodeposition also exist.[3,8,9] It is well documented that the synthesis processes[3,9–11] largely dictates the material properties of Zn_3N_2. For example, the first report on Zn_3N_2 synthesis described it as a black powder in 1940.[12] In contrast, techniques like MOCVD[1,13] and reactive sputtering[5,7,10] commonly results in stoichiometric Zn_3N_2 with cubic anti-bixbyite crystal structure and direct bandgap of 3.2 eV.

During the last decade, atomic later deposition (ALD) has emerged as a preferred technology for pin-hole free, conformal thin film deposition.[14,15] Its self-limiting growth characteristics provide good control over the films thickness. Though previously it was mostly used to deposit gate dielectrics,[14,16,17] lately it is being explored as an universal thin film deposition tool. Variety of materials including metals, composites, polymer and even thin films of hybrid materials[18,19] are deposited by ALD.

Different metal nitrides such as tantalum nitride,[20] tungsten nitride,[21] aluminum nitride,[22] molybdenum nitride,[23] titanium nitride[24] also have been reported by ALD using different metal precursors and ammonia or hydrazine as the nitrogen source. Recently, we have also reported the ALD of zinc nitride thin films[25] using diethylzinc (DEZ) and ammonia (NH_3) as the two ALD precursors.

In this paper, we report a detailed understanding of the atomistic mechanism occurring during the reaction of diethylzinc and ammonia, studied using density functional theory (DFT). Growth characteristics that follow the self-limiting deposition criteria are verified experimentally at 315 °C. As deposited films are found to be polycrystalline with preferential orientation along {321} direction. Promising performance of the ALD grown zinc nitride film as the channel layer in bottom-gate type TFTs is obtained.

2. Experimental details

2.1 Material deposition

Zinc nitride thin films were deposited in a hot wall viscous flow ALD reactor on quartz and Si substrates at 315 °C. Diethylzinc (DEZ; Aldrich) as the zinc source and ammonia (NH_3; 99.99994%) as the nitrogen source were used as precursors. Ultra high purity of N_2 gas was used as both carrier and purge gas. A continuous flow (200 sccm) of N_2 was used to keep the base pressure constant at 1 torr to ensure a laminar flow inside the reactor. Unless specified otherwise, the partial pressure of the DEZ and NH_3 exposure was kept at 0.05 and 1.6–2.0 torr s respectively. During the course of the film deposition, reactant exposure and purging time sequences were maintained by $m*t_1–t_2–n*t_3–t_4$. Here t_1 and t_3 are the pulsing time for DEZ and NH_3 dose, t_2 and t_4 are the purging time, set invariably to 40 s, while m and n are the number of exposures for DEZ and NH_3 respectively.

2.2 Reaction mechanism

DFT calculations were performed at room temperature to understand the atomistic reaction mechanism between diethylzinc and NH_3. Surface similar to the as grown ALD film was modelled using clusters representing the surface sites

[a]*Department of Energy Science and Engineering, IIT Bombay, Mumbai 400076, India. E-mail: shaibal.sarkar@iitb.ac.in; Fax: +91 22 2576 4890; Tel: +91 22 2576 7846*
[b]*Department of Chemistry, IIT Bombay, Mumbai 400076, India*

during proposed half surface reactions. All calculations were performed using Gaussian 09 [26] program with B3LYP functional[27,28] and a mixture of basis sets. LANL2 effective core potential and LANL2DZ basis set[28] was used to describe Zn while all other atoms were described using 6-31G basis set.[28–31] Structures corresponding to reactants, intermediate complex states, transition states and products were optimized and frequency calculations were carried out for locating and understanding the nature of the stationary points. All reported energies include the zero point energy obtained from calculations.

2.3 Material characterisations

The self-limiting behavior of the zinc nitride ALD for the DEZ exposure was examined by *ex situ* X-ray reflectivity (XRR) measurements. For thickness measurement, 400 ALD cycles of Zn_3N_2 was deposited on Si substrate at 315 °C. GlobalFit software was used to fit the experimentally acquired XRR data to obtain the film properties. Native SiO_2 on Si of thickness *ca.* 1–2 nm was taken into consideration into the model.

The crystal structure of the as deposited films was investigated by X-ray diffraction (XRD) pattern. For XRD measurement films with *ca.* 70 nm thickness were deposited on quartz substrates. The XRR and XRD measurements were carried out using Rigaku Smartlab X-ray diffractometer equipped with Cu-Kα source (1.54 Å).

Field emission scanning electron microscopy (SEM) was carried out in ZEISS Ultra-55 Scanning Electron Microscope to investigate the surface morphology of the deposited film. A film of 500 ALD cycles under saturated pulsing condition at 315 °C was grown on glass substrate for this purpose.

Optical property of the films deposited on glass substrates was studied by the UV-Vis absorption spectra measurement using PerkinElmer LAMBDA UV-Vis/NIR Spectrophotometers-950.

Electrical properties of the as deposited films were investigated with the Ecopia HMS-5000 Hall effect measurement system using van der Pauw four-point probe configuration. Approx. 50 nm of zinc nitride films were deposited on glass substrates for these measurements.

2.4 Fabrication of thin film transistor (TFT)

The bottom-gate configuration zinc nitride TFTs were fabricated on moderately conducting (<0.005 Ω cm) n-type Si substrate, which was also used as gate electrode. Fig. 1 shows the structural view of zinc nitride TFT. Si substrates were cleaned with IPA, rinsed in DI water, and blow-dried with N_2. The SiO_2 native oxide layer was removed by dipping the Si substrate in hydrofluoric acid (HF) solution prior to use.

300 nm thick Al_2O_3 was deposited on Si as gate insulating layer by ALD[32,33] at 250 °C using trimethylaluminum (TMA) and water (H_2O) as the two precursors for Al and O respectively. Zinc nitride film of *ca.* 50 nm thick was then deposited as the active channel layer on Al_2O_3/n-Si substrate at 315 °C under the saturated pulse condition. Following that, a wet etching process of zinc nitride and alumina was introduced to isolate the active device area. Dilute hydrochloric acid (HCl) and dilute hydrofluoric acid (HF) solutions were used for the wet etching of Zn_3N_2 and Al_2O_3 films respectively. Ag metal contacts were deposited through a shadow mask by thermal evaporation as source/drain top electrodes. The active channel layer of the Zn_3N_2 TFT had a width (W) of 3800 μm and a length (L) of 200 μm. The current–voltage characteristics of the TFT device were measured using a semiconductor parameter analyzer (Keithley, 4200-SCS).

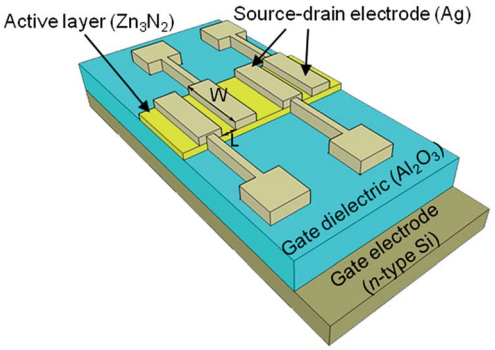

Fig. 1 A schematic diagram of Zn_3N_2 TFT with bottom-gate configuration.

3. Results and discussions

3.1 Study of the reaction chemistry by the DFT

Earlier reports of DFT calculations of various compounds have shown that calculated energies of reaction mechanisms were closely similar irrespective of the size of cluster used.[34–36]

The energy differences between calculations using large and small clusters have often found to be negligible. Thus, in order to keep our study simplistic, only smaller clusters are described here assuming larger clusters will provide similar results. $Zn(NH_2)_2$ and $Zn(C_2H_5)_2$ clusters were used to represent Zn–NH* and Zn–$CH_2CH_3^*$ reactive surface sites respectively for the two ALD half reactions.

The potential energy surface (PES) of $Zn(NH_2)_2$ and $Zn(C_2H_5)_2$ representing the 1st half reaction on Zn–NH* surface site is shown in Fig. 2(a). As seen from Fig. 2(a), DEZ (2) molecule first adsorbs on the Zn–NH* (1) surface site, in an exothermic reaction of −61.2 kJ mol^{-1} forming complex 1. Next, one ethyl group (–C_2H_5) of DEZ couples with a H atom of the –NH surface site through a transition state (TS1) with an activation barrier of 138.5 kJ mol^{-1} relative to the intermediate complex 1 to form ethylene (C_2H_6), which subsequently desorbs from the surface. The formation of the products [$NH_2ZnNH(ZnCH_2CH_3)$] (3) and C_2H_6 (4) of the proposed 1st half reaction has an exothermicity of 33.2 kJ mol^{-1} relative to the complex 1 formed. That the overall reaction is exothermic by 94.4 kJ mol^{-1} relative to the reactants suggest that the proposed half reaction is thermodynamically favourable.

The reaction of DEZ with Zn–NH* in the first half result in the formation of Zn–$CH_2CH_3^*$ surface sites which behaves as the starting point for the second half reaction. The second half reaction of NH_3 with [$ZnNH(C_2H_5)$]* proceeds in a similar mechanism as that of first half reaction depicted in the PES shown in Fig. 2(b). NH_3 adsorbs molecularly on a $Zn(C_2H_5)$*

surface site to form a complex (complex 2) in an exothermic reaction of 22.4 kJ mol^{-1}. The by-product of C_2H_6 is then formed by the transfer of a H atom from NH_3 to one C_2H_5 ligand with a barrier of 108.3 kJ mol^{-1} relative to the intermediate complex 2. This C_2H_6 subsequently desorbs resulting in an overall exothermic reaction of 91.5 kJ mol^{-1} relative to the reactants.

Single point energies calculated at the stationary points of the optimized structures thus result in thermodynamically favourable half surface reactions between DEZ and NH_3 acting as the Zn and N source respectively. The proposed deposition chemistry of zinc nitride ALD therefore can be expressed by the two separate surface limited half-reactions:[25]

$$\text{(A) } ZnNH_2^* + Et_2Zn \rightarrow ZnNHZnEt^* + C_2H_6$$

$$\text{(B) } ZnNHZnEt^* + NH_3 \rightarrow ZnNHZnNH_2^* + C_2H_6$$

The high barrier potential during each half surface reaction indicates the necessity of higher temperature to carry out film growth. Thus 315 °C deposition temperature reported here overcomes the large activation barrier during the reaction. It has also been found that the reaction between NH_3 and –NH* and that between DEZ and $-CH_3^*$ result in endothermicity with high activation barriers. High activation barriers during same surface site reactions were seen earlier in the DFT calculation of ALD silicon nitride as well.[36] Such reactions are thus thermodynamically and kinetically unstable demonstrating the self limiting nature of Zn_3N_2 ALD growth.

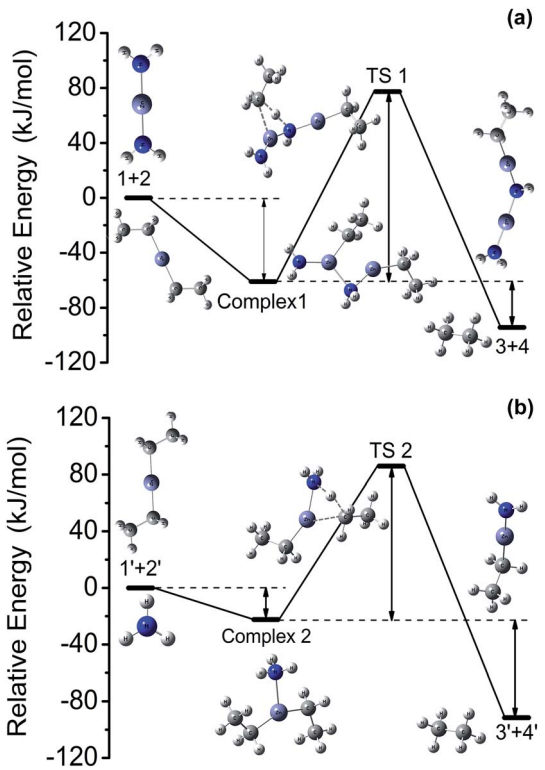

Fig. 2 (a) Reaction pathway and calculated energies for reaction of DEZ on Zn–NH* surface site. Calculations was done with $Zn(NH_2)_2$ cluster. The stationary points correspond to (1 + 2) Zn–NH + DEZ, (complex 1) $C_2H_5ZnC_2H_5$ complex, (TS1) C_2H_6 formation transition state and (3 + 4) $NH_2ZnNH-C_2H_5 + C_2H_6$ state. (b) Reaction pathways and calculated energies for reaction of NH_3 on $Zn-CH_3^*$ reaction surface site. $Zn(CH_3)_2$ cluster was used for calculations. The stationary points correspond to (1′ + 2′) $Zn-CH_2-CH_3 + NH_3$, (complex 2) NH_3 complex, (TS2) C_2H_6 formation transition state and (3′ + 4′) $C_2H_5ZnNH_2 + C_2H_6$ state.

3.2 Self-limiting behaviour study by the XRR measurement

Fig. 3 shows the growth rate per ALD cycle as a function of number of DEZ pulses with a constant 4 pulses of NH_3 exposure at 315 °C. As we reported earlier that the said dosage of NH_3 results in surface saturation.[25] To determine the film thickness, XRR measurements were performed. Fig. 3 (inset) shows a representative experimentally obtained Kiessig fringes along with the fitting for the film deposited with the pulse sequence as 1*1 s–40 s–4*1 s–40 s at 315 °C. It is clear that the growth rate per cycle initially increases with increasing number of DEZ doses and then reaches a plateau. Beyond this, any further increase of the reactant dosages has little effect on the net growth. This confirms the self-saturation behavior of the zinc nitride ALD for DEZ. Thus a saturated growth rate of *ca.* 0.9 Å per cycle was found with a ALD deposition sequence of 4*1 s–40 s–4*1 s–40 s.

3.3 Structural characterisation

Fig. 4(a) and (b) show the X-ray diffraction pattern of *ca.* 60 nm thick as deposited film grown at 315 °C under saturated dose condition. While the θ–2θ scan probes planes that are perpendicular to the substrate, on the contrary, the grazing angle incidence with parallel beam geometry mostly determine surface crystalline phases. Thus the combination of these two techniques is used here to determine the crystalline nature of the films.

The polycrystalline nature of the film is depicted in Fig. 4(a). Peaks at 31.7, 34.3, 36.6, 39, 43.3, 47.4, 56.5, 63 and

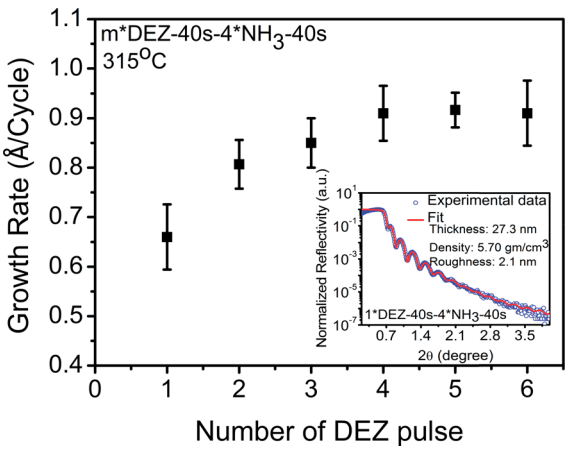

Fig. 3 Growth rate per cycle as a function of number of DEZ pulses for constant number of NH_3 pulses (self-limiting characteristics) for the zinc nitride ALD at 315 °C. (Inset) X-ray reflectivity measurement data and fitting of the film grown on Si substrate with (1, 4) pulse sequence.

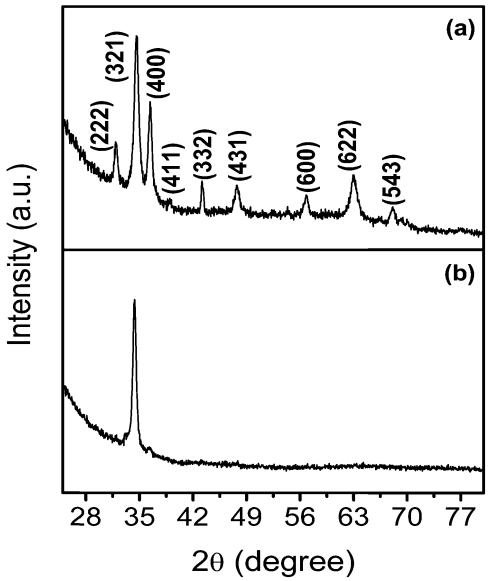

Fig. 4 X-ray diffraction patterns (a) grazing angle, (b) θ–2θ of zinc nitride thin films deposited on quartz substrate at 315 °C substrate temperatures.

67.8° corresponding to the (222), (321), (400), (411), (332), (431), (600), (622) and (543) planes respectively of cubic zinc nitride agrees with the JCPDS file (Card no. 00-035-0762). The θ–2θ scan, Fig. 4(b), reveals the out of plane orientation along {321} direction. We can thus infer that the as deposited films are polycrystalline with preferred orientation along {321} direction.

The surface morphology of the zinc nitride film deposited on glass substrate at the same conditions which was used to grow the channel layer for the bottom-gate TFT is showed in Fig. 5. The film was grown at 315 °C with the saturated condition of both the ALD precursors. It is clear from the surface SEM image that the film was uniform and pinhole free and also having a less identified grain boundary. This can make a positive impact on the electrical properties of the zinc nitride as channel layer.

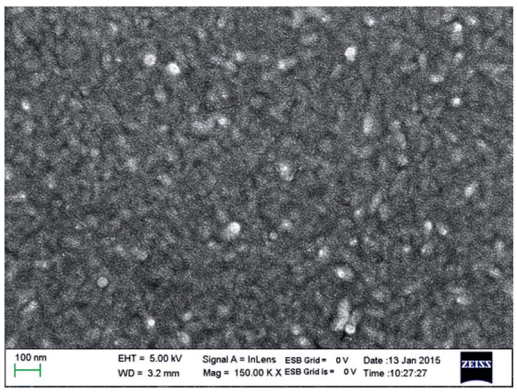

Fig. 5 Surface SEM image of the zinc nitride film used as channel layer in bottom-gate configuration was grown on glass substrate.

3.4 Optical properties

Fig. 6 shows the absorption spectrum of a 50 nm thick zinc nitride film deposited on glass substrate at 315 °C with the saturation pulsing condition. The film shows a high transparency in the wide range of visible light.

The optical bandgap of the material is found to be *ca.* 3.1 eV as calculated from the Tauc plot, as shown in the inset of the Fig. 6.

3.5 Electrical properties

Electrical properties of the as deposited films were studied with standard Hall measurements in ambient condition at room temperature. The as grown Zn_3N_2 films showed n-type conductivity with carrier concentration in the order of 10^{18} cm^{-3}. The Hall mobility and resistivity of the material was found to be *ca.* 4–6 $cm^2 V^{-1} s^{-1}$ and *ca.* 10^{-3} Ω cm respectively. Since the resistivity depends highly on the thickness, all electrical measurements were performed on film with thickness *ca.* 50 nm deposited on glass substrates.

3.6 Characteristics of the zinc nitride TFT

Bottom-gate TFT was fabricated on moderately conducting Si substrates that in turn also served as the back contact of the device. For gate dielectric we used 300 nm of ALD grown Al_2O_3, deposited inside the same reactor. ALD grown Zn_3N_2 channel layer of *ca.* 50 nm thickness was deposited under saturated dose condition at 315 °C. Two Ag metal contacts were deposited as source and drain electrode. Fig. 7(a) shows the output characteristics, *i.e.* drain current (I_{DS}) *vs.* drain to source voltage (V_{DS}), of the as fabricated transistor with channel length and width of 200 μm and 3800 μm respectively. This device clearly shows saturation characteristics under varied gate to source voltage. At $V_{GS} = 0$ V, there is a non-negligible current that flows through the channel under varying V_{DS}. This reflects and confirms the high carrier concentration in the channel. Therefore hereinafter we operate the transistor only under depletion-mode.

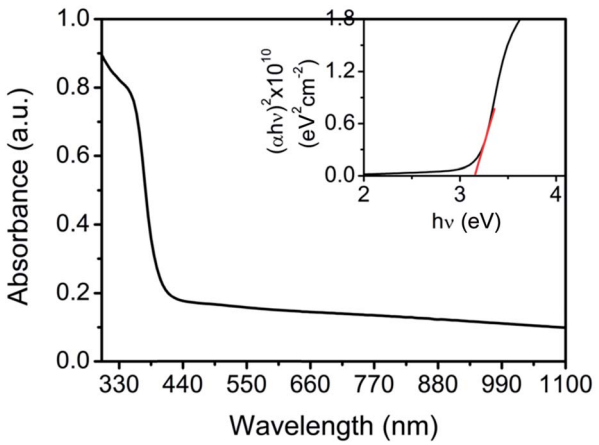

Fig. 6 Absorption spectrum of the ALD grown zinc nitride film on glass substrate deposited at 315 °C. Inset: Tauc plot for the bandgap determination.

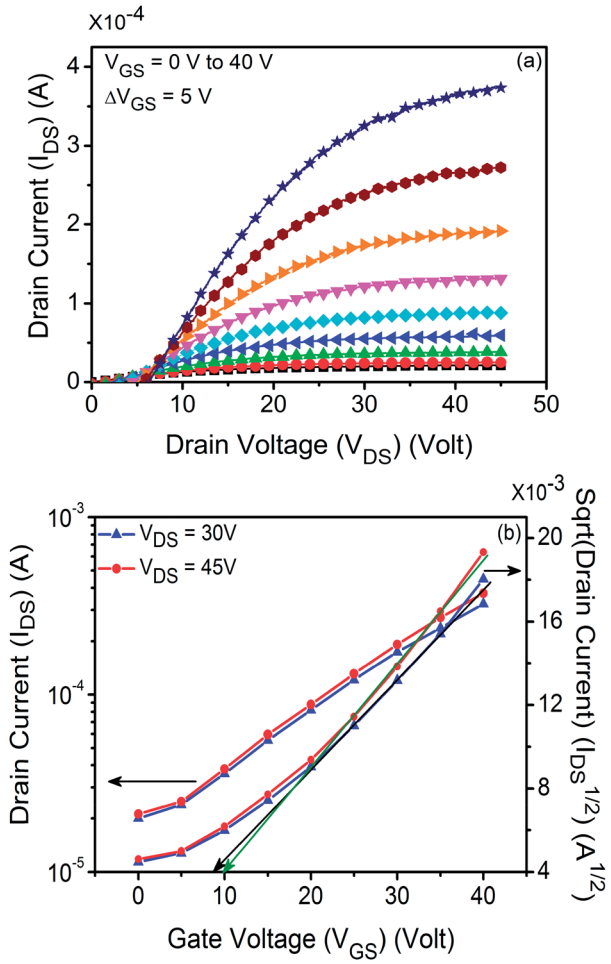

Fig. 7 Electrical characteristics of Zn_3N_2 TFT: (a) output characteristics obtained from the TFT with a W/L = 3800/200 for V_{GS} varying from 0 to 40 Volts and (b) transfer characteristics of the TFT with a W/L = 3800/200 at V_{DS} = 30 Volts and 45 Volts.

The field effect mobility (μ_{FE}) of the Zn_3N_2 channel layer was estimated from the TFT characteristics using the following equation for the operation of the transistor in the saturation region:[2,37,38]

$$I_{DS,sat} = \frac{W}{L}\mu_{FE}C_{Al_2O_3}\frac{(V_{GS} - V_{th})^2}{2} \quad (1)$$

where $C_{Al_2O_3}$ is the capacitance per unit area of the insulating Al_2O_3 layer. The $C_{Al_2O_3}$ of 300 nm thick Al_2O_3 layer was calculated as 27 nF cm^{-2} using the relation $C_{Al_2O_3} = \varepsilon_{Al_2O_3}/d$, ($\varepsilon_{Al_2O_3} = \varepsilon_r \times \varepsilon_0 = 9 \times 8.854 \times 10^{-12}$ F m^{-1}),[37,39,40] where d is the thickness and ε_r is the dielectric constant (or relative permittivity) of the Al_2O_3 insulating layer and ε_0 is free space permittivity. Here we assumed the dielectric constant value of the ALD grown Al_2O_3 at 250 °C, to be 9.[39–40]

To determine the threshold voltage (V_{th}), the transistor transfer characteristics curve, as shown in the Fig. 7(b), was derived from the output characteristics curve. The square root of drain current ($I_{DS}^{1/2}$) at constant drain to source voltage (V_{DS} = 30 V and 45 V) was shown as a function of varying gate bias voltage (V_{GS}) along with the drain current (I_{DS}). The threshold voltage (V_{th}) was calculated by fitting a straight line to the plot of $I_{DS}^{1/2}$ *versus* V_{GS} at the constant V_{DS} of 30 Volts and 45 Volts respectively. The derived V_{th} is *ca.* 9.8–10 Volts as shown in the Fig. 7(b).

At V_{DS} = 45 V and V_{GS} = 40 V, the $I_{DS,sat}$ value is found to be 370 μA. Hence using eqn (1), the field effect mobility (μ_{FE}) of the channel layer is obtained to be 1.6 cm^2 V^{-1} s^{-1}. Noteworthy here; the calculated field effect mobility (μ_{FE}) is found similar to the one derived from the Hall measurement (μ_{Hall} = 5 cm^2 V^{-1} s^{-1}) though there was a little difference between the measured and calculate value of mobility which may be due to the leakage current from the gate through the dielectric layer which also reported by Núñez *et al.*[2]

4. Conclusions

Strongly oriented polycrystalline Zn_3N_2 films were deposited by sequential exposure of DEZ and NH_3 at 315 °C. The deposition follows the self-limiting growth characteristics. The reaction mechanism and the reaction pathway were studied using density functional theory based calculation.

As deposited films were optically transparent (E_g = 3.1 eV) and n-type in nature. A bottom gate thin film transistor was fabricated by ALD which showed an n-channel depletion-mode output characteristic with *ca.* 1.6 cm^2 V^{-1} s^{-1} field effect mobility of the channel layer.

Acknowledgements

The authors thank the National Centre for Photovoltaic Research and Education (NCPRE) aided by the Ministry of New and Renewable Energy, Govt. of India, for financial support. We thank Azaj Ansari for his help in DFT calculation.

Notes and references

1 T. Suda and K. Kakishita, *J. Appl. Phys.*, 2006, **99**, 076101.
2 C. G. Núñez, J. L. Pau, E. Ruíz and J. Piqueras, *Appl. Phys. Lett.*, 2012, **101**, 253501.
3 K. Toyoura, H. Tsujimura, T. Goto, K. Hachiya, R. Hagiwara and Y. Ito, *Thin Solid Films*, 2005, **492**, 88.
4 C. García Núñez, J. L. Pau, M. J. Hernández, M. Cervera and J. Piqueras, *Appl. Phys. Lett.*, 2011, **99**, 232112.
5 Y. Naoomi, W. Kouki, Y. Takahiro, S. Atsushi and N. Yoshihiko, *Jpn. J. Appl. Phys.*, 2014, **53**, 05FX01.
6 D. S. Ginley and C. Bright, *MRS Bull.*, 2000, **25**, 15.
7 E. Aperathitis, V. Kambilafka and M. Modreanu, *Thin Solid Films*, 2009, **518**, 1036.
8 T. Goto, K. Toyoura, H. Tsujimura and Y. Ito, *Mater. Sci. Eng., A*, 2004, **380**, 41.
9 K. Kuriyama, Y. Takahashi and F. Sunohara, *Phys. Rev. B: Condens. Matter Mater. Phys.*, 1993, **48**, 2781.
10 F. Zong, H. Ma, W. Du, J. Ma, X. Zhang, H. Xiao, F. Ji and C. Xue, *Appl. Surf. Sci.*, 2006, **252**, 7983.
11 M. Futsuhara, K. Yoshioka and O. Takai, *Thin Solid Films*, 1998, **322**, 274.

12 R. Juza and H. Hahn, *Z. Anorg. Allg. Chem.*, 1940, **244**, 125.
13 D. Wang, Y. C. Liu, R. Mu, J. Y. Zhang, Y. M. Lu, D. Z. Shen and X. W. Fan, *J. Phys.: Condens. Matter*, 2004, **16**, 4635.
14 P. F. Carcia, R. S. McLean and M. H. Reilly, *Appl. Phys. Lett.*, 2006, **88**, 123509.
15 S. J. Lim, J. M. Kim, D. Kim, S. Kwon, J. S. Park and H. Kim, *J. Electrochem. Soc.*, 2010, **157**, H214.
16 C. M. Tanner, Y.-C. Perng, C. Frewin, S. E. Saddow and J. P. Chang, *Appl. Phys. Lett.*, 2007, **91**, 203510.
17 X.-H. Zhang, B. Domercq, X. Wang, S. Yoo, T. Kondo, Z. L. Wang and B. Kippelen, *Org. Electron.*, 2007, **8**, 718.
18 K. B. Klepper, O. Nilsen, P.-A. Hansen and H. Fjellvag, *Dalton Trans.*, 2011, 4636.
19 K. B. Klepper, O. Nilsen, T. Levy and H. Fjellvåg, *Eur. J. Inorg. Chem.*, 2011, **2011**, 5305.
20 B. B. Burton, A. R. Lavoie and S. M. George, *J. Electrochem. Soc.*, 2008, **155**, D508.
21 J. S. Becker, S. Suh, S. L. Wang and R. G. Gordon, *Chem. Mater.*, 2003, **15**, 2969.
22 R. L. Puurunen, M. Lindblad, A. Root and A. O. I. Krause, *Phys. Chem. Chem. Phys.*, 2001, **3**, 1093.
23 D. K. Nandi, U. K. Sen, D. Choudhury, S. Mitra and S. K. Sarkar, *ACS Appl. Mater. Interfaces*, 2014, **6**, 6606.
24 J. Musschoot, Q. Xie, D. Deduytsche, S. Van den Berghe, R. L. Van Meirhaeghe and C. Detavernier, *Microelectron. Eng.*, 2009, **86**, 72.
25 S. Sinha and S. K. Sarkar, *RSC Adv.*, 2014, **4**, 47177.
26 M. J. Frisch, G. W. Trucks, H. B. Schlegel, G. E. Scuseria, M. A. Robb, J. R. Cheeseman, G. Scalmani, V. Barone, B. Mennucci, G. A. Petersson, H. Nakatsuji, M. Caricato, X. Li, H. P. Hratchian, A. F. Izmaylov, J. Bloino, G. Zheng, J. L. Sonnenberg, M. Hada, M. Ehara, K. Toyota, R. Fukuda, J. Hasegawa, M. Ishida, T. Nakajima, Y. Honda, O. Kitao, H. Nakai, T. Vreven, J. A. Montgomery Jr, J. E. Peralta, F. Ogliaro, M. J. Bearpark, J. Heyd, E. N. Brothers, K. N. Kudin, V. N. Staroverov, R. Kobayashi, J. Normand, K. Raghavachari, A. P. Rendell, J. C. Burant, S. S. Iyengar, J. Tomasi, M. Cossi, N. Rega, N. J. Millam, M. Klene, J. E. Knox, J. B. Cross, V. Bakken, C. Adamo, J. Jaramillo, R. Gomperts, R. E. Stratmann, O. Yazyev, A. J. Austin, R. Cammi, C. Pomelli, J. W. Ochterski, R. L. Martin, K. Morokuma, V. G. Zakrzewski, G. A. Voth, P. Salvador, J. J. Dannenberg, S. Dapprich, A. D. Daniels, Ö. Farkas, J. B. Foresman, J. V. Ortiz, J. Cioslowski and D. J. Fox, *R. D. Gaussian 09*, Gaussian, Inc., Wallingford, CT, USA, 2009.
27 C. T. Lee, W. T. Yang and R. G. Parr, *Phys. Rev. B: Condens. Matter Mater. Phys.*, 1988, **37**, 785.
28 A. D. Becke, *J. Chem. Phys.*, 1993, **98**, 5648.
29 P. J. Hay and W. R. Wadt, *J. Chem. Phys.*, 1985, **82**, 299.
30 P. J. Hay and W. R. Wadt, *J. Chem. Phys.*, 1985, **82**, 270.
31 W. R. Wadt and P. J. Hay, *J. Chem. Phys.*, 1985, **82**, 284.
32 S. M. George, *Chem. Rev.*, 2010, **110**, 111.
33 C. A. Wilson, R. K. Grubbs and S. M. George, *Chem. Mater.*, 2005, **17**, 5625.
34 Y. Widjaja and C. B. Musgrave, *Appl. Phys. Lett.*, 2002, **80**, 3304.
35 Y. Xu and C. B. Musgrave, *Chem. Mater.*, 2004, **16**, 646.
36 C. Mui, Y. Widjaja, J. K. Kang and C. B. Musgrave, *Surf. Sci.*, 2004, **557**, 159.
37 K. Semyung, B. Seokhwan, L. Seungjun, J. Sunyeol, J. Wooho, K. Hyungchul, G. Su Cheol, C. Ho Jung, P. Hyung-ho and J. Hyeongtag, *Semicond. Sci. Technol.*, 2009, **24**, 035015.
38 S. Masuda, K. Kitamura, Y. Okumura, S. Miyatake, H. Tabata and T. Kawai, *J. Appl. Phys.*, 2003, **93**, 1624.
39 G. D. Wilk, R. M. Wallace and J. M. Anthony, *J. Appl. Phys.*, 2001, **89**, 5243.
40 M. D. Groner, J. W. Elam, F. H. Fabreguette and S. M. George, *Thin Solid Films*, 2002, **413**, 186.